# CHAPTER II
# LITERATURE REVIEW

## 2.1 Azo Dyes

### 2.1.1 General Remarks

The term of "azo dyes" is applied to those synthetic organic colorants that are characterized by the presence of the chromophoric azo group (–N=N–). This divalent group is attached to $sp^2$ hybridized carbon atom on one side and to an aromatic or heterocyclic nucleus on the other. It may be linked to an unsaturated molecule of the carboxylic, heterocyclic, or aliphatic type. No natural dyes contain this chromophore. Commercially, the azo dyes are the largest and most versatile class of organic dyestuffs. There are more than 10,000 Color Index (CI) generic names assigned to commercial colorants, where approximately 4,500 are in use, and over 50% of these belong to the azo class. Synthetic dyes are derived in whole or in part from cyclic intermediates. Approximately two-thirds of the dyes are used by the textile industry to dye natural and synthetic fibers or fabrics, about one-sixth is used for coloring paper, and the rest is used chiefly in the production of organic pigments and in the dyeing of leather and plastic. Dyes are sold as pastes, powders, and liquids with concentrations varied from 6 to 100 %. The concentration, form, and purity of a dye are determined largely by the use, for which it is intended.

### 2.1.2 Classification and Designations

The most authoritative compilation covering the constitution, properties, preparations, manufactures, and other coloring data is the publication of Color Index, which is edited jointly by the Society of Dyers and Colorists and the American Association of Textile Chemists and Colorists (AATCC). In the Color Index, a dual classification system is employed to group dyes according to area of usage and chemical constitution. Because of the ease of applications, azo dyes comprise the largest chemical class in numbers, monetary value, and tonnage produced. There are more than 2,200 chemical structures of azo dyes disclosed in the Colour Index.

Nearly all dye manufactures use letters and numerals in the name of their products to define the color. For example, B is blue; G, yellow (gelb in German) or green; R, red; and Y, yellow. Numerals, i.e. 2G (or GG), 3G, 4G, etc. indicate, in this case, a successively yellower or greener shade. Occasionally, suffixed letters are used to feature other properties, such as solubility, light fastness, brightness, and use on synthetic fibers.

Chemically, the azo class is subdivided according to the number of azo groups present into mono-, dis-, tris-, tetrakis-, etc. Mono- and diazo dyes are essentially equal in importance, trisazo dyes are less important, and tetrakisazo dyes, except for a few, are much less important. For this reason, substances with more than three azo linkages are generally included under the heading of polyazo dyes. Table 2.1 lists the Color Index of the azo dyes.

**Table 2.1** Color Index of different azo dyes (Mary, 1991)

| Chemical class | Color Index number range |
|---|---|
| Monoazo | 11,000 – 19,999 |
| Diazo | 20,000 – 29,999 |
| Trisazo | 30,000 – 34,999 |
| Polyazo | 35,000 – 36,999 |

## 2.2 Semiconductor

A semiconductor is a material with an electrical conductivity that is intermediate between that of an insulator and a conductor. Like other solids, semiconductor materials have electronic band structure determined by the crystal properties of the material. A semiconductor used as photocatalyst should be an oxide or sulfide of metals, such as $TiO_2$, CdS, and ZnO. The actual energy distribution among electrons is described by the Fermi level and temperature of the electrons. At absolute zero temperature, all of the electrons have energy below the Fermi energy, but at non-zero temperature, the energy levels are randomized, and some electrons have energy above the Fermi level.

Among the bands filled with electrons, the one with the highest energy level is referred to as the valence band, and the band outside of this is referred to as the conduction band. The energy width of the forbidden band between the valence band and the conduction band is referred to as the band gap. The overall structure of band gap energy is shown in Figure 2.1.

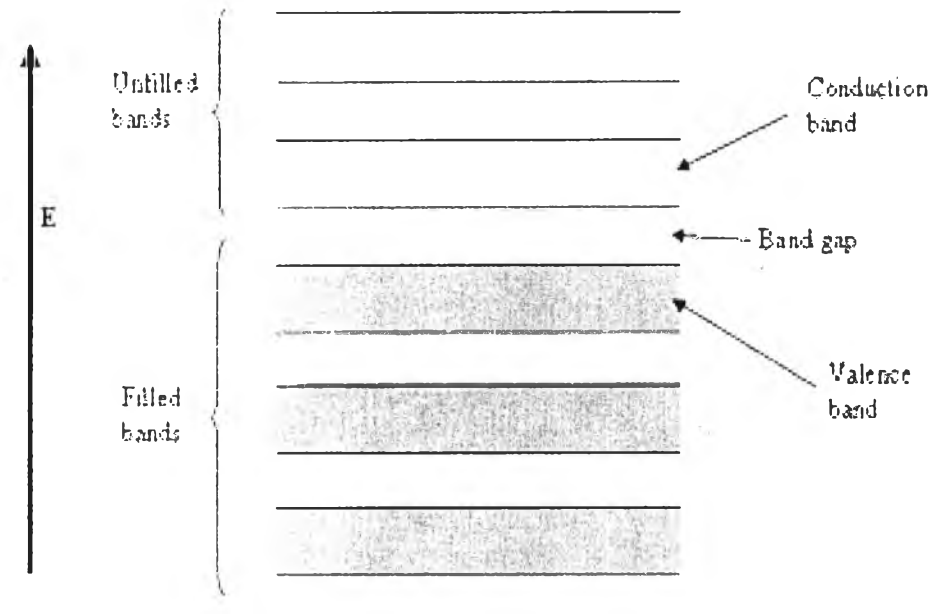


**Figure 2.1** The structure of band gap energy.

The band gap can be considered as a wall that electrons must jump over in order to become free. The amount of energy required to jump over the wall is referred to as the band gap energy ($E_g$). Only electrons that jump over the wall and enter the conduction band (CB) can move around freely. When light is illuminated at appropriate wavelengths with energy equal or more than band gap energy, valence band (VB) electrons can move up to the conduction band (CB). At the same time, as many positive holes as the number of electrons that have jumped to the conduction band (CB) are created. The valence band (VB), conduction band (CB), band gap, and band gap wavelength of some common semiconductors are shown in Table 2.2.

**Table 2.2** The band gap positions of some common semiconductor photocatalysts (Robertson, 1996; and Vali, 2007)

| Semiconductor | Valence band (eV) | Conduction band (eV) | Band gap (eV) | Band gap wavelength (nm) |
|---|---|---|---|---|
| $TiO_2$ | +3.1 | -0.1 | 3.2 | 387 |
| $SnO_2$ | +4.1 | +0.3 | 3.8 | 326 |
| $SrZrO_3$ | +4.3 | -1.3 | 5.6 | 221 |
| ZnO | +3.0 | -0.2 | 3.2 | 387 |
| ZnS | +1.4 | -2.3 | 3.7 | 335 |
| $WO_3$ | +3.0 | +0.2 | 2.8 | 443 |
| CdS | +2.1 | -0.4 | 2.5 | 496 |
| CdSe | +1.6 | -0.1 | 1.7 | 729 |
| GaAs | +1.0 | -0.4 | 1.4 | 886 |
| GaP | +1.3 | -1.0 | 2.3 | 539 |

## 2.3 Photocatalysts

### 2.3.1 Titanium Dioxide ($TiO_2$)

Titanium dioxide ($TiO_2$) is a wide band gap semiconductor that has been extensively investigated and applied to a wide spectrum of chemical disciplines. Its uses are, for instances, in selective oxidation and reduction, polymerization, condensation reaction, substitutional fluorination of olefins and phosphates, photovoltaics, and in photo degradation of organic and inorganic compounds (Fox and Chen, 1981). The high photoactivity, thermal and chemical stability, low cost, and non-toxicity of $TiO_2$ make it a good candidate for such applications. $TiO_2$ is found in three crystalline phases: anatase, rutile, and brookite, as well as in an amorphous phase. The anatase phase has a band gap energy of 3.2 eV, the rutile phase of 3.0 eV, and the brookite phase of 3.4 eV at room temperature. (Hoffmann *et al.*, 1995). This corresponds to maximal wavelength absorptions ranging from 365 to 413 nm. Upon illumination of the $TiO_2$ with light of equal or greater energy than its band gap energy, charge transfer from valence band to conduction band occurs,

creating a hole ($h^+$) and a free electron ($e^-$). These species can either recombine or migrate to the surface and react with surface-bound adsorbates, typically oxygen or water in most photo-oxidative processes. Since UV light makes up of less than 5 % of the solar spectrum that reaches the earth's surface, the commercial application of these processes has been limited. However, a large degree of characterization works has been accomplished to date.

The main four polymorphs of $TiO_2$ found in nature are anatase (tetragonal), brookite (orthorhombic), rutile (tetragonal), and $TiO_2$ (B) (monoclinic). The structures of rutile, anatase, and brookite can be discussed in terms of ($TiO_2^{6-}$) octahedrals. The three crystal structures differ by the distortion of each octahedral and by the assembly patterns of the octahedral chains. Anatase can be regarded to be builtup from octahedrals that are connected by their vertices; in rutile, the edges are connected; and in brookite, both vertices and edges are connected, as shown in Figure 2.2 (Carp *et al.*, 2004).

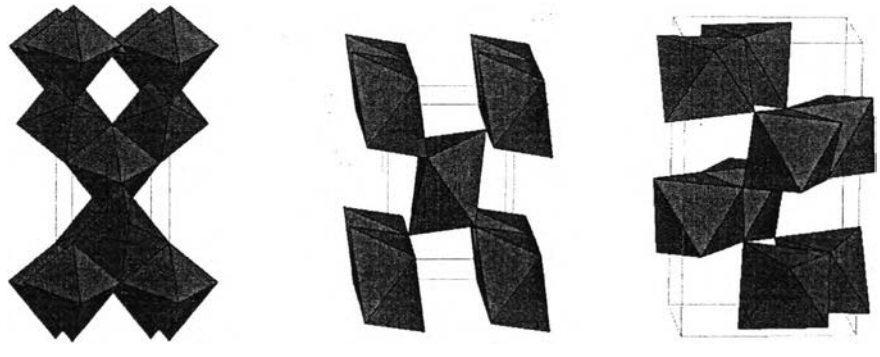

(a) (b) (c)

**Figure 2.2** Crystal structures of (a) anatase, (b) rutile, and (c) brookite.

In photocatalysis applications, both crystal structures, i.e. anatase and rutile, are commonly used, with anatase showing a greater photocatalytic activity for most reactions. It has been suggested that this increased photoreactivity is due to anatase's slightly higher Fermi level, lower capacity to adsorb oxygen, and higher degree of hydroxylation (i.e. number of hydroxyl groups on the surface). Reactions, in which both crystalline phases have the same photoreactivity (Deng *et al.*, 2002) or

rutile a higher one (Mills *et al.*, 2003), are also reported. Furthermore, there are also studies, which claim that a mixture of anatase (70-75 %) and rutile (30-25 %) is more active than pure anatase (Mugglie and Ding, 2001). The disagreement of the results may lie in the intervening effect of various coexisting factors, such as specific surface area, pore size distribution, crystal size, and preparation methods, or in the way the activity is expressed. The behavior of Degussa P-25 commercial $TiO_2$ photocatalyst, consisting of a mixture of anatase and rutile in an approximate proportion of 80/20, is for many reactions more active than both the pure crystalline phases. The enhanced activity arises from the increased efficiency of the $e^-/h^+$ separation due to the multiphase nature of the particles.

As a semiconductor, $TiO_2$ functions by having a large band gap, which can be described as an energy threshold that electrons must obtain in order to flow through a material. The band gap is located between the filled valence band and the higher energy conduction band. The magnitude between the electronically occupied valence band and the largely unpopulated conduction band determines both the extent of thermal population of the conduction band (i.e. the electrical conductivity of the material) and the wavelength sensitivity of the semiconductor to irradiation. That is, a material with a larger band gap requires higher energy radiation to populate the conduction band than one with a smaller band gap.

The general mechanism for photocatalytic reaction on semiconductor $TiO_2$ can be explained as shown in Figure 2.3. The absorption of light in $TiO_2$ at the wavelengths of less than 387 nm (for the anatase crystal with the band gap of 3.2 eV) leads to the promotion of an electron from the valence band to the conduction band of the semiconductor. This excitation process creates an electron in the conduction band and an electron vacancy (a hole) in a valence band. The electron-hole pairs that are generated in this way migrate toward the surface where they can initiate the redox reactions with absorbates. Because the valence band edge of $TiO_2$ is located at approximately +3.2 eV with respect to a normal hydrogen electrode (NHE) at pH 0 (the position of the band edge is pH-dependent), these holes are very powerful oxidizing agents and are capable of oxidizing a variety of organic molecules, leading to the formation of mainly $CO_2$ and $H_2O$. However, the main issue to be taken into

consideration is that $TiO_2$ photocatalyst can only be exited by UV light because of their wide band gap.

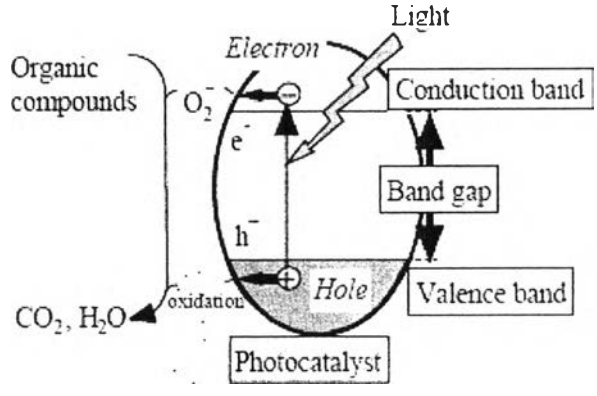


**Figure 2.3** Mechanism of photocatalysis.

2.3.2 Doping of $TiO_2$

When applied to semiconductor, the term *doping* refers to the intentional introduction of impurities to the material for the purpose of modifying electrical characteristics. With the above depiction of semiconduction in mind, an ideal dopant must increase the valence band edge, thus reducing the band gap without lowering the conduction band, and either improve or at least minimize electron-hole recombination, so as to minimize any loss in quantum yield. It also should not impart any instability, have thermal or chemical stability, and optimally be inexpensive to apply.

A number of methods have been investigated and found to narrow the band gap of $TiO_2$. A common method, used successfully for solar cell applications, is accomplished by attaching various organic dyes, such as ruthenium complexes, to the surface (Hoffmann *et al.*, 1995). Unfortunately, this method is expensive, and such dyes degrade in the presence of oxygen. Ruthenium dyes also cannot be used in aqueous solutions as they can be readily washed off from the surface. Reduction of $TiO_2$ via hydrogenation has also been investigated. This method does narrow the band gap, allowing visible light for activation, but at the expense of lowering the conduction band, thus reducing the photocatalytic reduction power of the system. Another method available to narrow the band gap is to dope the semiconductor with

metals and non-metals. Most transition and rare earth metals have been investigated. Metals, such as $Fe^{3+}$, $Mo^{5+}$, $Rh^{3+}$, $V^{4+}$, and $Ru^{3+}$, have been found to tune the electronic structure of $TiO_2$ and improve its photocatalytic activity in the visible range. However, these methods require either expensive ion-implantation facilities or suffer from thermal instability and low quantum yields due to the continuum of inter band states found in transition metals. Doping with anionic non-metals, such as N, S, C, I, P, and B, has also been reported (Ding and Liu, 1998).

### 2.3.3 Indium Oxide and Silver Dopants

Indium oxide ($In_2O_3$) has been extensively reported as one of the most interesting oxide, and a great number of applications have been reported, such as in the development of solar cells, photovoltaic and optoelectronic devices, and liquid crystal displays (Gopchandran *et al.*, 1997). $In_2O_3$ is a semiconductor that has been demonstrated to increase the photocatalytic and photoelectron chemical responses of semiconductor oxide by reducing energy band gap, enhancing electron transfer, and reducing recombination of the photocatalytic charge carriers. It can absorb light of wavelengths shorter than 480 nm with the band gap of ~2.5 eV. Therefore, $In_2O_3$ dopant is beneficial to improve the photoactivity of $TiO_2$ due to decreasing its band gap.

Silver is also an extremely attractive metal to be investigated as a dopant due to its remarkable catalytic activity and its size-and-shape dependent optical properties (Yang *et al.*, 2008). In the photocatalytic applications, metallic Ag can prevent $e^-$-$h^+$ pairs from fast recombination owing to its strong electron trap ability, resulting in enhanced quantum efficiency of the photocatalysts. For this purpose, $Ag/TiO_2$ photocatalysts have been extensively studied (Cozzoli *et al.*, 2004). Co-doping of $TiO_2$ with $In_2O_3$ and Ag has been consideraed to present a new three-component junction photocatalytic system, and the co-operation of $In_2O_3$ and Ag is expected to lead to an enhanced photocatalytic activity compared with $Ag/TiO_2$ or $In_2O_3/TiO_2$ two-component junction systems.

Shchukin *et al.* (2004) reported that nanocrystalline bicomponent $TiO_2$-$In_2O_3$ powders with various Ti/In ratios have been prepared by a sol–gel technique and calcined at 473 and 723 K. Their crystalline structure, surface area, surface acidity, sorption properties with respect to 2-chlorophenol, and optical absorption were determined by appropriate techniques (XRD, BET, FTIR, and UV-Vis spectroscopies), while their photocatalytic activity (PCA) was tested in the case of the degradation of 2-chlorophenol in water. For both calcination temperatures, PCA increased with decreasing $In_2O_3$ content, reaching a maximum at ca. 10 wt.% of $In_2O_3$. For this latter sample and the one containing 20 wt.% $In_2O_3$, PCA was greatly enhanced with respect to $TiO_2$, especially for the sample pretreated at 473 K. The concentration of the main aromatic intermediate products (chlorohydroquinone and catechol) was considerably lower for $TiO_2$-$In_2O_3$ photocatalysts than for pure $TiO_2$. On the basis of various characterisations of the photocatalysts, the reasons invoked to explain the PCA enhancement due to $In_2O_3$ include a better separation of photogenerated charge carriers, an improved oxygen reduction, and an increased surface acidity inducing a higher extent of adsorption of the aromatics.

Yang *et al.* (2008) reported that a novel co-doped $TiO_2$ photocatalyst, $Ag/In_2O_3$–$TiO_2$, was developed through a one-step sol–gel process followed by a solvent thermal treatment in the presence of triblock copolymer surfactant. The product showed very small particle size (12 ± 2 nm) with metallic Ag clusters well-distributed on the surface of the product. At the same time, the product was mainly in the anatase phase with high crystallinity. The photocatalytic activity of $Ag/In_2O_3$–$TiO_2$ was evaluated by the degradation of an aqueous solution of Rhodamine B (RB) dye, and the obtained significantly high photocatalytic activity can be ascribed to the simultaneous effects of doped Ag by acting as electron-trapping site and semiconductor $In_2O_3$ as band gap-narrowing sensitizer. In addition, the unique morphology and nanosize of the product also played an important role in this enhanced photocatalytic activity.

Yang *et al.* (2008) reported that the metallic Ag and semiconductor $In_2O_3$-codoped $TiO_2$ nanocomposites ($Ag/In_2O_3$-$TiO_2$), which were prepared by a one-step sol-gel-solvothermal method in the presence of a triblock copolymer surfactant (P123), showed an enhanced photocatalytic activity. The resulting $Ag/In_2O_3$-$TiO_2$ three-component systems mainly exhibited an anatase phase structure, high crystallinity, and extremely small particle sizes with metallic Ag particles well-distributed on the surface. Compared with pure anatase $TiO_2$, the $Ag/In_2O_3$-$TiO_2$ systems showed narrowing of the band gap energy due to the change in the band position caused by the contribution of the In 5s5p orbits to the conduction band. By tuning Ag or $In_2O_3$ loading and molar ratio of titanium source to the surfactant, size and dispersion of the product particles can be controlled. As-prepared $Ag/In_2O_3$-$TiO_2$ nanocomposites were used as the photocatalysts to degrade Rhodamine B (RB) dye and methyl ter-butyl ether (MTBE) in the liquid phase. At 2.0 % Ag and 1.9 % $In_2O_3$ dopes, the $Ag/In_2O_3$-$TiO_2$ system exhibited the highest UV light photocatalytic activity, and nearly total degradation of RB dye (25 mg/l) or MTBE (200 mg/l) was obtained after 45 or 120 min UV light irradiation. In addition, the UV light photocatalytic activity of the three-component systems exceeded that of the single ($TiO_2$) and two-component ($Ag/TiO_2$ or $In_2O_3$-$TiO_2$) systems, as well as the commercial photocatalyst, Degussa P25.

Wang *et al.* (2009) reported the preparation of $TiO_2$ doped with indium using a sol-gel method, in which titanium (IV) tetrabutaxide and indium chloride were used as precursors. They revealed a unique chemical species, O-In-$Cl_x$ ($x$ = 1 or 2), existed on the surface of the indium-doped $TiO_2$. The surface state energy level attributed to the surface O-In-$Cl_x$ species was located at 0.3 eV below the conduction band of $TiO_2$. The transition of electrons from the valence band of $TiO_2$ to the surface state energy level was responsive to visible light. The photogenerated carriers generated under visible light irradiation can be efficiently separated by the surface state energy level of the O-In-$Cl_x$ species and the valence band of $TiO_2$ to contribute to the photocatalytic reaction. Consequently, the indium-doped $TiO_2$ showed an improved photocatalytic activity for photodegradation of 4-chlorophenol compared to pure $TiO_2$ under visible light irradiation.

## 2.4 Nano-Photocatalysts

### 2.4.1 General Remarks

Nanocrystalline photocatalysts are ultra-small semiconductor particles, which are few nanometers in size. During the past decade, the photochemistry of nanosized semiconductor particles has been one of the fastest growing research areas in physical chemistry. The interest in these small semiconductor particles originates from their unique photophysical and photocatalytic properties. Several review articles have been published concerning the photophysical properties of nanocrystalline semiconductors. Such studies have demonstrated that some properties of nanocrystalline semiconductor particles are in fact different from those of bulk materials.

Nanosized particles possess properties with falling into the region of transition between the molecular and bulk phases. In the bulk material, the electron excited by light absorption funds a high density of states in the conduction band, where it can exist with different kinetics energies. In the case of nanoparticles, however, the particle size is the same as or smaller than the size of the first excited state. Thus, the electrons and holes generated upon illumination cannot suit into such a particle, unless they assume a state of higher kinetics energy.

Hence, as the size of the semiconductor particle is reduced below a critical diameter, the spatial confinement of the charge carriers within a potential well, like ''a particle in a box'', causes them to mechanically behave quantum. In solid state terminology, this means that the bands split into discrete electronic states (quantized levels) in the valence and conduction bands, and the nanoparticle progressively behaves similar to a giant atom. Nanosized semiconductor particles, which exhibit size-dependent optical and electronic properties, are called quantized particles or quantum dots (Kamat, 1995).

### 2.4.2 Activity of Nano-Photocatalysts

One of the main advantages of the application of nanosized particles is the increase in the band gap energy with decreasing particle size. As the size of a semiconductor particle falls below the critical radius, the charge carriers begin to

behave mechanically quantum, and the charge confinement leads to a series of discrete electronic states. As a result, there is an increase in the effective band gap and a shift of the band edges. Thus by varying the size of the semiconductor particles, it is possible to enhance the redox potential of the valence band holes and the conduction band electrons.

However, the solvent reorganizational free energy for charge transfer to a substrate remains unchanged. The increasing driving force and the unchanged solvent reorganizational free energy are expected to lead to an increase in the rate constants for charge transfer at the surface. The use of nanosized semiconductor particles may result in an increased photocatalytic activity for systems, in which the rate-limiting step is interfacial charge transfer. Hence, nanosized semiconductor particles can possess enhanced photoredox chemistry with reduction reactions, which might not otherwise proceed in bulk materials, being able to occur readily using sufficiently small particles. Another factor, which could be advantageous, is the fact that the fraction of atoms that are located at the surface of a nanoparticle is very large. Nanosized particles also have high surface area-to-volume ratios, which further enhances their catalytic activity. One disadvantage of nanosized particles is the need for light with a shorter wavelength for photocatalyst activation. Thus, a smaller percentage of a polychromatic light source will be useful for photocatalysis.

## 2.5 Photocatalytic Decomposition Mechanisms

### 2.5.1 Photocatalytic Oxidation

It is well established that conduction band electrons ($e^-$) and valence band holes ($h^+$) are generated when aqueous $TiO_2$ suspension is irradiated by light with energy greater than its band gap energy ($E_g$, 3.2 eV). The photogenerated electrons can reduce the dye or react with electron acceptors, such as $O_2$ adsorbed on the Ti(III)-surface or dissolved in water, reducing it to superoxide radical anion, $O_2^{\bullet-}$. The photogenerated holes can oxidize the organic molecule to form $R^+$ or react with $OH^-$ or $H_2O$, oxidizing them into $OH^\bullet$ radicals. Together with other highly oxidant species (peroxide radicals), they are reported to be responsible for the heterogeneous $TiO_2$ photodecomposition of organic substrates, such as dyes. According to this, the

relevant reactions at the semiconductor surface causing the decomposition of dyes can be expressed as follows:

$$TiO_2 + h\nu(UV) \rightarrow TiO_2(e_{CB}^- + h_{VB}^+) \quad (1)$$

$$TiO_2(h_{VB}^+) + H_2O \rightarrow TiO_2 + H^+ + OH^\bullet \quad (2)$$

$$TiO_2(h_{VB}^+) + OH^- \rightarrow TiO_2 + OH^\bullet \quad (3)$$

$$TiO_2(e_{CB}^-) + O_2 \rightarrow TiO_2 + O_2^{\bullet -} \quad (4)$$

$$O_2^{\bullet -} + H^+ \rightarrow HO_2^\bullet \quad (5)$$

$$Dye + OH^\bullet, HO_2^\bullet, O_2^{\bullet -} \rightarrow \text{decomposition products} \quad (6)$$

$$Dye + h_{VB}^+ \rightarrow \text{oxidation products} \quad (7)$$

$$Dye + e_{CB}^- \rightarrow \text{reduction products} \quad (8)$$

The resulting $OH^\bullet$ radical, being a very strong oxidizing agent (standard redox potential of +2.8 V), as well as $HO_2^\bullet$ and $O_2^{\bullet -}$, can oxidize most of azo dyes to the mineral end-products. Substrates not reactive toward hydroxyl radicals are decomposed employing $TiO_2$ photocatalysis with rates of decay highly influenced by the semiconductor valence band edge position. The role of reductive pathways (Equation (8)) in heterogeneous photocatalysis has been envisaged also in the decomposition of several dyes but in a minor extent than oxidation.

### 2.5.2 Photosensitized Oxidation

The mechanism of photosensitized oxidation (called also photoassisted decomposition) by visible radiation ($\lambda > 420$ nm) is different from the pathway implicated under UV light radiation. In the former case, the mechanism suggests that excitation of the adsorbed dye takes place by visible light to appropriate singlet or triplet states, subsequently followed by electron injection from the excited dye molecule into the conduction band of the $TiO_2$ particles, whereas the dye is converted to the cationic dye radicals ($Dye^{\bullet +}$) that undergoes decomposition to yield products as follows:

$$Dye + hv(visible) \rightarrow {}^1Dye^* \text{ or } {}^3Dye^* \quad (9)$$

$${}^1Dye^* \text{ or } {}^3Dye^* + TiO_2 \rightarrow Dye^{\bullet +} + TiO_2(e_{CB}^-) \quad (10)$$

$$TiO_2(e_{CB}^-) + O_2 \rightarrow O_2^{\bullet -} + TiO_2 \quad (11)$$

$$Dye^{\bullet +} \rightarrow \text{decomposition products} \quad (12)$$

The cationic dye radicals readily react with hydroxyl ions, undergoing oxidation via Equations (13) and (14), or interact effectively with $O_2^{\bullet-}$, $HO_2^{\bullet}$, or $HO^{\bullet-}$ species to generate intermediates that ultimately lead to $CO_2$ (Equations (15) – (19)).

$$Dye^{\bullet+} + OH^- \rightarrow Dye + HO^{\bullet} \quad (13)$$

$$Dye + 2HO^{\bullet} \rightarrow H_2O + \text{oxidation products} \quad (14)$$

$$O_2^{\bullet-} + H^+ \rightarrow HO_2^{\bullet} \quad (15)$$

$$HO_2^{\bullet} + H^+ + TiO_2(e_{CB}^-) \rightarrow H_2O_2 + TiO_2 \quad (16)$$

$$H_2O_2 + TiO_2(e_{CB}^-) \rightarrow HO^{\bullet} + HO^- + TiO_2 \quad (17)$$

$$Dye^{\bullet+} + O_2^{\bullet-} \rightarrow DO_2 \rightarrow \text{decomposition products} \quad (18)$$

$$Dye^{\bullet+} + HO_2^{\bullet}(\text{or } HO^{\bullet}) \rightarrow \text{decomposition products} \quad (19)$$

When using sunlight or simulated sunlight (laboratory experiments), it is suggested that both photooxidation and photosensitizing mechanisms occur during the irradiation, and both $TiO_2$ and the light source are necessary for the reaction to occur. In the photocatalytic oxidation, $TiO_2$ has to be irradiated and excited in a near-UV energy to induce charge separation. On the other hand, dyes rather than $TiO_2$ can be excited by visible light followed by electron injection into $TiO_2$ conduction band, which leads to photosensitized oxidation. It is difficult to conclude whether the photocatalytic oxidation is superior to the photosensitizing oxidation mechanism, but the photosensitizing mechanism will help improve the overall efficiency and make the photobleaching of dyes using solar light more feasible.

## 2.6 Factors Influencing Photocatalytic Degradation of Dyes

### 2.6.1 Effect of Initial Dye Concentration

Yao *et al.* (2004) studied the decomposition of methyl orange by bismuth titanate, $Bi_4Ti_3O_{12}$, thin film prepared by using the chemical solution decomposition (CSD) method. The results showed that with different methyl orange concentrations varied from 5 to 20 mg/l, the decomposition efficiency decreased with increasing concentration of methyl orange. The strong decrease in the observed rate constants with the increase in initial dye concentration was attributed to the significant absorption of light by the substrate in the same wavelength range of photocatalyst excitation. For increasing the initial methyl orange concentration, the

photon flow reaching the photocatalyst particles decreased due to the fact that with increasing aliquots, photons are absorbed by the methyl orange molecules present in the solution and/or on the photocatalyst surface. Moreover, this dependence can also be related to the formation of several layers of adsorbed dye on the photocatalyst surface, which is higher at higher dye concentrations. The large amount of adsorbed dye inhibits the reaction of dye molecules with photogenerated holes or hydroxyl radicals because of the increased distance between reactants and photocatalysts.

### 2.6.2 Effect of Solution pH

The heterogeneous photocatalysis has been found to be pH dependent. Yao *et al.* (2004) also showed that with different initial pH values (1.22, 2.43, 5.18, 7.13, 10.2, and 12.7), the reaction rate increased under acidic pH but decreased under alkaline pH. The effect of pH on the decomposition of the pollutants is variable and controversial. The increase in decomposition rate under acidic pH was explained on the basis that at low pH, $HO_2$ radicals will form, and this will compensate for the effect of decreasing hydroxyl ion concentration. The decrease in decomposition rate at alkaline pH is assumed to be due to the anions and the highly negative charged oxide surface, and the decomposition would, thus, depend on diffusion of surface-generated $OH^{\bullet}$ towards the inside layer to the low concentration of methyl orange anion, a slower process than direct charge transfer.

### 2.6.3 Effect of Light Intensity and Irradiation Time

Oillis *et al.* (1991) reviewed the studies reported for the effect of light intensity on the kinetics of the photocatalysis process and stated that (i) at low light intensities (0–20 $mW/cm^2$), the rate would increase linearly with increasing light intensity (first order), (ii) at intermediate light intensities beyond a certain value (approximately 25 $mW/cm^2$), the rate would depend on the square root of the light intensity (half order), and (iii) at high light intensities, the rate is independent of light intensity. This is likely because at low light intensity, reactions involving electron–hole formation are predominant, and electron–hole recombination is negligible. However, when increasing light intensity, electron–hole pair separation competes with recombination, thereby causing lower effect on the reaction rate. It is evident

that the percentage of decolorization and degradation increases with an increase in irradiation time. The reaction rate decreases with irradiation time since it follows apparent first-order kinetics, and additionally a competition for decomposition may occur between the reactant and the intermediate products. The slow kinetics of dye decomposition after certain time limit is due to:

- The difficulty in converting the N-atoms of dye into oxidized nitrogen compounds
- The slow reaction of short chain aliphatics with $OH^{\bullet}$ radicals
- The short life-time of photocatalyst

because of active site deactivation by strong by-product adsorption (Konstantinou and Albanis, 2004).

### 2.6.4 Effect of $H_2O_2$ Addition

The influence of the strong oxidant species additives, such as $H_2O_2$, has been in some case controversial, and it appeared strongly dependent on substrate type and on various experimental parameters. Their usefulness should be accurately checked under each operative condition.

Yao *et al.* (2004) studied the decomposition of methyl orange and showed that with different concentrations of $H_2O_2$ (0, 0.1, and 1 mol/l), when the $H_2O_2$ was added, a significant increase in decomposition rate was noted for methyl orange decomposition but must be in the presence of photocatalyst and light irradiation. Moreover, partial decomposition was observed for methyl orange under irradiation of the homogeneous systems in the presence of $H_2O_2$. In their work, the highest decomposition rate was achieved with 0.1 M $H_2O_2$ added. The added $H_2O_2$ contributed to the reactive radical intermediates ($OH^{\bullet}$) formed from the oxidants by reaction with the photogenerated electrons, which can exert a dual function: as strong oxidant themselves and as electron scavengers, thus inhibiting the electron–hole recombination at the semiconductor surface.

2.6.5 Effect of Calcination Temperature of Photocatalyst

Yao *et al.* (2004) studied the effect of different calcination temperatures of photocatalyst for 5 min (400, 500, 600, and 700°C) at the same concentration of methyl orange (10 mg/l). The results showed that the photocatalytic activity of photocatalyst had no significant difference among the calcination temperatures of 400, 500, and 600°C, but the photocatalytic activity of the prepared photocatalysts was significantly reduced at higher calcination temperature (700°C).

Zhang *et al.* (2004) studied the photocatalytic activity of ZnO–$SnO_2$ for decomposition of methyl orange, and the effect of heat treating at different calcination temperatures was investigated (300, 350, 400, 450, 500, 600, 700, 800, and 900°C). The results showed that the degradation rate of methyl orange was increased with increasing calcination temperature except for 300°C because of the partial formation of crystallite oxides. With increasing calcination temperature, the size of crystallite oxides increases, contributing to the increase in photocatalytic activity. However, at temperatures higher than 700°C, the photocatalyst exhibited poor activity because of the negative effect of the coupled oxides.

2.6.6 Effect of Calcination Time of Photocatalyst

Yao *et al.* (2004) also studied the effect of calcination time on the photocatalytic activity of the prepared bismuth titanate photocatalyst thin film calcined at 600°C. The results showed that at 1 min of calcination time, the highest decomposition of methyl orange was obtained. While the rate constant increased with increasing calcination temperature, but at calcination time of 5 min, the rate constant reached the highest value because at the higher calcination time of 10 min, the sintering of photocatalyst material occurred.

## 2.7 Porous Materials

The classification of pores according to size has been under discussion for many years, but in the past, the terms ''micropore'' and ''macropore'' have been applied in different ways by physical chemists and some other scientists. In an attempt to clarify this situation, the limits of size of the different categories of pores

included in Table 2.3 have been proposed by the International Union of Pure and Applied Chemistry (IUPAC), (Ishizaki *et al.*, 1988 and Rouquerol *et al.*, 1999). As indicated, the ''pore size'' is generally specified as the ''pore width'', i.e. the available distance between the two opposite walls. Obviously, pore size has a precise meaning when the geometrical shape is well defined. Nevertheless, for most purposes, the limiting size is that of the smallest dimension, and this is generally taken to represent the effective pore size. Micropores and mesopores are especially important in the context of adsorption.

**Table 2.3** Definitions about porous solids

| Term | Definition |
|---|---|
| Porous solid | Solid with cavities or channels which are deeper than they are wide |
| Micropore | Pore of internal width less than 2 nm |
| Mesopore | Pore of internal width between 2 and 50 nm |
| Macropore | Pore of internal width greater than 50 nm |
| Pore size | Pore width (diameter of cylindrical pore or distance between opposite walls of slit) |
| Pore volume | Volume of pores determined by stated method |
| Surface area | Extent of total surface area determined by given method under stated conditions |

According to the IUPAC classification, porous materials are regularly organized into three categories on a basis of predominant pore size as follows:

- Microporous materials (pore size < 2 nm) include amorphous silica and inorganic gel to crystalline materials, such as zeolites, aluminophosphates, gallophosphates, and related materials.
- Mesoporous materials (2 nm ≤ pore size ≤ 50 nm) include the M41S family (e.g. MCM-41, MCM-48, MCM-50, etc.) and other non-silica materials synthesized via intercalation of layered materials, such as double hydroxides,

metal (titanium, zirconium) phosphates, and clays.

- Macroporous materials (pore size > 50 nm) include glass-related materials, aerogels, and xerogels.

Nowadays, micro- and mesoporous materials are generally called ''nanoporous materials''. Particularly, mesoporous materials are remarkably very suitable for catalysis applications, whereas the pores of microporous materials may become easily plugged during catalyst preparation if high metal loading is required.

## 2.8 Sol-Gel Process

The sol-gel process has been intensively studied because it is so effective to prepare nano-sized mesoporous materials (Sreethawong *et al.*, 2005). Because the metal oxides can be deactivated due to sintering or crystal growth during their continuous use in high temperature processes, and the photocatalytic performance of the metal oxides is well-known to depend on their specific surface area, sol-gel method presents some particular advantages through a low-temperature process, avoiding contamination of the materials. It also yields better stoichiometric control and the possibility of grain-size and grain-shape control. This technique does not require complicated instruments, such as in chemical vapor deposition method. It provides a simple and easy means of synthesizing nano-sized particles, which is essential for nano-photocatalysts. It involves the formation of metal-oxo-polymer network from molecular precursors, such as metal alkoxides, and subsequent polycondensation, as follows:

$$\text{M-OR} + \text{H}_2\text{O} \rightarrow \text{M-OH} + \text{ROH} \quad (20)$$

$$\text{M-OH} + \text{M-OR} \rightarrow \text{M-O-M} + \text{R-OH} \quad (21)$$

$$\text{M-OH} + \text{M-OH} \rightarrow \text{M-O-M} + \text{H}_2\text{O} \quad (22)$$

where M = Ti, Si, Zr, Al, and R = alkyl group.

All stages, including the formation of colloid particles to form gel network, drying of wet gel, and calcination stage, can all lead to grain growth and formation of agglomerates. Hence, to carefully control the process is very essential in preparing high-performance and high-reliability powders. The relative rates of hydrolysis and polycondensation strongly influence the structure and properties of the resulting

metal oxides. Typically, sol-gel-derived precipitates are amorphous in nature, requiring further heat treatment to induce crystallization. The calcination process frequently gives rise to particle agglomeration and grain growth, and may induce phase transformation (Wang and Ying, 1999). Thus, a surfactant is used to prevent agglomeration of the particle. The $BaTiO_3$ nanoparticles synthesized by sol-gel process (Yu *et al.*, 2008), however, are easy to form agglomeration. This can be avoided by the application of the surfactant, i.e. oleic acid, as cheap and innoxious surfactant, thus preventing the agglomeration of particles. The sol-gel process by the addition of surfactant can help enforce size controllability and prepare well-dispersed powders. The ideal model of forming the $BaTiO_3$ is shown in Figure 2.4 .

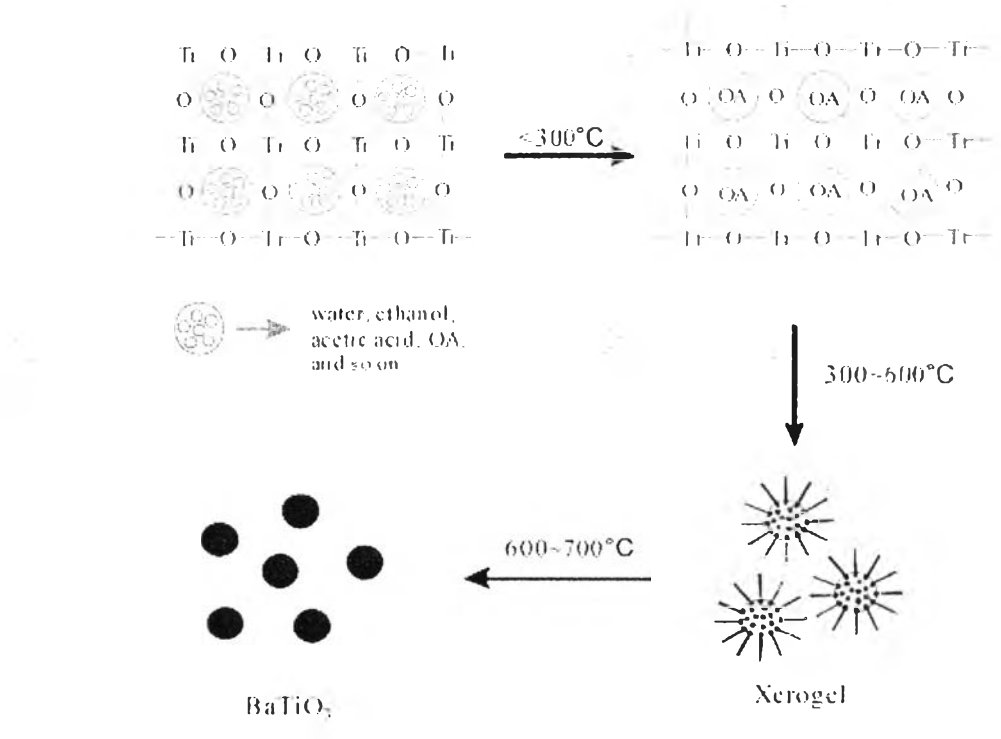


**Figure 2.4** A schematic of forming the $BaTiO_3$ nanoparticles (Yu *et al.*, 2008).

The process can be divided to three steps. Firstly, oleic acid (OA) enchases in the 3D network structure of -Ti-O-Ti- when the temperature is lower than 300°C. Secondly, between 300 and 600°C, a number of "microcapsules" of $BaTiO_3$ precursors coated by OA are formed. The carboxyl of OA is towards the inside and

hydrophobic -R group towards the outside. Excessive OA as solution will allow the system to form "microcapsules". Finally, when the temperature is higher than 600°C, OA decomposes, and the walls of "microcapsules" are destroyed. Although this happens, the shape of $BaTiO_3$ precursor is preserved, thus producing better-dispersed $BaTiO_3$ nanoparticles.

Factors affecting the sol-gel process include the reactivity of metal alkoxides, pH of the reaction medium, water-to-alkoxide ratio, reaction temperature, and nature of solvent and additive. The water-to-alkoxide ratio governs the sol-gel chemistry and the structural characteristics of the hydrolyzed gel. High water-to-alkoxide ratio in the reaction medium ensures a more complete hydrolysis of alkoxides, favoring nucleation versus particle growth. In addition, an increase in water-to-alkoxide ratio leads to reducing the crystallite size of the calcined catalyst. An alternative approach to control the sol-gel reaction rates involves the use of acid or base catalyst. It was reported that for a system with a water-to-alkoxide ratio of 165, the addition of HCl resulted in the reduction of the crystallite size from 20 to 14 nm for materials calcined at 450°C. Besides, a finer grain size and a narrower pore size distribution with a smaller average pore diameter were also attained for the sample synthesized with HCl (Wang and Ying, 1999). The size of alkoxide group also plays an important role in controlling the particle size. The titanium alkoxide containing bulky groups, such as titanium amiloxide, reduces the hydrolysis rate, which is advantageous for the preparation of fine colloidal particles (Murakami *et al.*, 1999).